Journal of
Applied Remote Sensing

RemoteSensing.SPIEDigitalLibrary.org

Determining soil water content of salt-affected soil using far-infrared spectra: laboratory experiment

Lu Xu
Zhichun Wang
Maina John Nyongesah
Gang Liu

SPIE.

Determining soil water content of salt-affected soil using far-infrared spectra: laboratory experiment

Lu Xu,[a,b,*] Zhichun Wang,[c] Maina John Nyongesah,[d] and Gang Liu[e]

[a]Chinese Academy of Sciences, Xinjiang Institute of Ecology and Geography, 818 Road Beijing, Urumqi 830011, China

[b]University of Chinese Academy of Sciences, Beijing, 19 Road Yuquan, Beijing 100049, China

[c]Chinese Academy of Sciences, Northeast Institute of Geography and Agroecology, 4888 Shengbei Street, Changchun 130012, China

[d]Jaramogi Oginga Odinga University of Science and Technology, Bondo, 210-40601, Kenya

[e]Shizuoka University, Graduate School of Agriculture, 836 Ohya, Shizuoka 422-8529, Japan

Abstract. Rapid determination of soil water content is urgently needed for monitoring and modeling ecosystem processes and improving agricultural practices, especially in arid landscapes. Far-infrared band application in soil water measurement is still limited. Various samples were arranged to simulate complex field condition and emissivity was obtained from a Fourier transform infrared spectrometer. Four spectral forms (including raw spectra, logarithm of reciprocal spectra, first-order derivate, and second-order derivate) were employed to develop a partial least squares regression model. The results indicate that the model with first-order derivate spectral form was identified with the highest performance ($R^2 = 0.87$ and root mean square error = 1.88%) at the range of 8.309 to 10.771 μm. Judging from the contribution of the bands to each principal component, the band region from 8.27 to 9.112 μm holds a great promise for soil water content estimation. Several channels of ASTER and MODIS correspond to the involved band domain, which show the potential of predicting and mapping soil water content on large scales. However, there are still constraints due to the differences in spectral resolution between instrument and sensors and the influence of complex factors under field conditions, which are still challenges for forthcoming studies. [DOI: 10.1117/1.JRS.9.095983]

Keywords: soil water content; saline soil; far-infrared spectra; emissivity; partial least square regression; arid land.

Paper 15500 received Jul. 16, 2015; accepted for publication Nov. 3, 2015; published online Dec. 9, 2015.

1 Introduction

Soil water content is an important factor in the exchange of energy and mass between the atmosphere and the earth surface.[1,2] It also plays a critical role in crop productivity, especially in arid regions.[3,4] Although traditional techniques have been applied for measuring soil water content, they are time-consuming, laborious, and only provides point data.[5] Therefore, timely and accurate estimation of soil water content is urgently required for irrigation schedule management and environmental studies.

Remote sensing affords a direct approach to map the spatial distribution of soil characteristics for continuous temporal coverage at regional and global scales.[6] Numerous studies have shown huge progress in soil water evaluation based on remote sensing methods,[7–11] where spectral bands from optical to microwave regions have been investigated for soil water content determination. Bowers and Hanks[8] measured a range of soils and found a decrease in reflectance with increasing moisture content. Neema et al.[12] pointed out that soil reflectance decreased with soil water content increasing up to a certain level and then increased with higher moisture content. They also proposed a new concept of cut-off thickness, defined as the thickness of soil that

*Address all correspondence to: Lu Xu, E-mail: 573270714@qq.com

1931-3195/2015/$25.00 © 2015 SPIE

transmits 5% of incident light only. Moran et al.[13] and Gillies et al.[14] presented a method of using vegetation indices and surface temperatures to estimate crop water deficit, which could translate to soil water. Liu et al.[15] and Whiting et al.[16] found that shortwave-infrared region was suitable for predicting soil water as well.

Meanwhile, efforts are being made in microwave radiation because of its superior ability to penetrate into the soil and, in some wavelengths, to penetrate through the vegetation cover.[3,17] Passive microwave remote sensing has a great potential in modeling soil water retrieval for its all-time and all-weather capability and frequent coverage,[18] while active sensors offer possibilities of high spatial resolution (10 m for synthetic aperture radar).[1] Wang and Schmugge[19] developed a dielectric constant model to calculate soil water content. Jackson and Schmugge[20] applied L-band (~1.4 GHz) to assess topsoil water over a wide range of vegetated conditions. Bindlish and Barros[21] combined active and passive microwave remote sensing data to assess soil water and considered the spatial heterogeneity effect. Mao et al.[22] employed AMSR-E data and vertical polarized microwave index for assessing soil water on the Tibetan Plateau.

Most of these studies focused on the visible, near-infrared, short-wave infrared, and microwave wavelength region, while studies on the far-infrared wavelength domain are limited.[23] Carlson et al.[24,25] explored relationships among soil water content, surface temperature (ST), and normalized difference vegetation index (NDVI), and then lead many studies of soil water content estimation with ST and NDVI, where ST was extracted from far-infrared wavelength region.[26,27]

Salt-affected soil is common in arid areas. Soil salt and soil water jointly affect spectra and cause huge anomalies in predicting soil salinity or moisture content.[28] Farifteh[29] found it difficult to accurately evaluate soil salinity or soil water content under field conditions where soil was influenced by both salt and moisture. Further progress in hyperspectra was made by Wang et al.,[30] who developed salt-resistant hyperspectral indices for estimating soil water content in arid landscapes. However, limited research is available in far-infrared region.

With the development of remote sensing, multisource data and their application have emerged.[31,32] The progress of statistical methods has advanced a step further as well through partial least squares regression (PLSR), multivariate adaptive regression splines, artificial neural networks, and so on.[31–33] The PLSR algorithm can model several response variables simultaneously and also effectively deal with collinear and noisy independent variables.[34] Additionally, numerous studies have demonstrated successful outcomes and potential applications of PLSR in various domains.[35,36] Owing to the spectra covering thousands of generally collated wavelengths, cross-validation has been used often to eliminate the overfitting problem associated with other regression methods.[37] Furthermore, numerous studies have suggested that variation in forms of original data is very helpful for data-mining, such as first-order derivative, second-order derivative, and continuum removal.[38–40] These techniques are more robust and hence preferred in the current study.

The current study determined far-infrared spectral data with a Fourier transform infrared (FTIR) spectrometer from various levels of artificial soil water content from the same salt-affected soil. Based on four spectral forms and actual measurement of soil water content, the PLSR model will be built up to estimate soil water content of saline soil and, ultimately, a new model will be developed to trace soil water content. The specific aims are (1) to verify statistical relationship between soil water content and various forms of far-infrared spectra and (2) to select feature bands and establish a PLSR model for soil water estimation of saline soils.

2 Materials and Methods

2.1 *Experiment Arrangement*

The soil sampling site is located at a typical inland river basin in the west of China. Annual precipitation, evaporation, temperature, and relative humidity in the region are 187 mm, 1841.9 mm, 6.6°C, and 58%, respectively.[41] Topsoil (0 to 20 cm) samples were collected for laboratory analysis. The soil samples were air-dried for several weeks and sieved through

two sieves of 0.2 and 2 mm to make three groups of soil sample with different particle sizes to simulate different soil surface roughness. To produce a great diversity and randomness of soil water content, 30 top-opened cylinder containers in 15 cm diameter and 10 levels of height from 1 to 10 cm were prepared for these soil samples. Thus, each group consisted of 10 samples with 10 soil column sample heights.

Chemical properties of the three types of resampled soil were analyzed via an extracted solution, which was made from a mixture of soil and distilled water with the ratio of 1:5. The properties of the resampled soil are presented in Table 1.

Gravimetric method was applied to estimate soil water content. Distilled water was added gently and evenly to all the 30 samples using a watering can to avoid destroying the soil surface. Addition of water was stopped when soil water content reached 20%. After this, natural drying process began. Due to various soil types of particle and soil column sample heights, each sample had evaporation rate different from the others and would have different soil water content, which could simulate more complex field conditions. During the process, soil radiance and soil water content of each sample were synchronously measured five times in time sequence, and the measurement dates and times are shown in Table 2.

2.2 *Emissivity Measurement and Spectra Forms*

Soil radiances were measured with Design and Prototypes Inc. Model 102 FTIR spectrometer.[42] The core of the spectrometer is the Michelson interferometer, which contains infrared optics, beam splitter, and a scanning mirror assembly. The light passes through the interferometer onto an infrared detector that consists of indium antimonide and mercury cadmium telluride. This detector set has a spectral range of ~2 to 16 μm. The standard input optic is 2.54 cm in diameter with a 4.8 deg expanding field of view, which gives a 7-cm-diameter spot at ~70 cm height. The instrument was set up with a spectral resolution of 4 cm^{-1} and scanned to COADD with number of eight. For each measurement of radiance, three raw data were obtained, including warm blackbody (WBB), cold blackbody (CBB), and sample intensity. The sample radiance could be calculated with sample intensity calibrated by WBB and CBB, and also each sample temperature was obtained. To enlarge the temperature difference between sample and environment, and to obtain gradient variations of soil water content at the same time, soil samples were heated to ~303 K using a quartz tungsten halogen lamp. The measurement was basically carried out in a dark room. Due to the noise of environment

Table 1 Soil properties of different particles from Sangong River basin.

Sample	pH	Electrical conductivity (mS/cm)	Total salt (mg/g)	Cl^- (mg/g)	SO_4^{2-} (mg/g)	Ca^{2+} (mg/g)	K^+ (mg/g)	Mg^{2+} (mg/g)	Na^+ (mg/g)	CO_3^{2-} (mg/g)	HCO_3^- (mg/g)
>2 mm	8.64	4.86	22.70	0.05	13.08	1.64	0.20	0.05	5.11	0.00	0.18
0.2 to 2 mm	8.70	5.79	27.20	0.03	15.69	1.65	0.20	0.05	6.47	0.00	0.18
0 to 0.2 mm	8.40	6.27	29.40	0.04	16.40	2.09	0.20	0.05	6.96	0.00	0.14

Table 2 The measurement sequence and corresponding time.

Measurement sequence	Soil water content= 20%	1st	2nd	3rd	4th	5th
Measurement date and time	August 5, 2013 3:00 a.m.	August 6, 2013 11:00 p.m.	August 7, 2013 9:30 p.m.	August 9, 2013 10:30 p.m.	August 13, 2013 5:30 p.m.	August 27, 2013 10:00 p.m.
Hours after (h)	0	44	67	115	206	547

Note: 1st, 2nd, 3rd, 4th, and 5th represent the times measured soil water content and radiance.

and instrument, the method of five points moving average was used to eliminate the noise signal.[43]

Radiance of a black body is governed by Planck's law with the sample temperature.

$$B(\lambda, T) = \frac{c1}{\lambda^5 (e^{c2/\lambda T} - 1)}, \tag{1}$$

where the unit is $\mathrm{mW}/(\mathrm{m}^2 \times \mathrm{ster} \times \mu\mathrm{m})$, λ is wavelength in cm, T is the temperature of emitting surface in K, $c1 = 1.191044 \times 10^{-5}$ $[\mathrm{mW}/(\mathrm{m}^2 \times \mathrm{ster} \times \mathrm{cm}^{-4})]$, and $c2 = 1.438769$ (cm K).

Due to some measuring deficiencies, we applied relative emissivity by correcting the absolute values with the average value of 7 to 7.5 μm, which has emissivity close to 1. Such data treatment may cause some deviations, but as long as spectra patterns rather than absolute values are focused on, as in this study, it may not deviate very much from the real patterns. Hence, relative emissivity (rE) was computed as

$$\mathrm{rE} = \frac{R_{\mathrm{sam}}}{R_{\mathrm{B}}}, \tag{2}$$

where rE is the relative emissivity, R_{sam} is the radiance of sample, and R_{B} is the radiance of a black body with the sample temperature.

Based on the relative emission spectra (rE), logarithm of reciprocal spectra (LRE), first-order derivative spectra (DE), and second-order derivative spectra (DDE) were calculated as follows:

$$\mathrm{LRE} = \log_{10}\mathrm{RE}; \quad \mathrm{RE} = \frac{1}{\mathrm{rE}}, \tag{3}$$

$$\mathrm{DE} = \frac{\mathrm{rE}(\lambda + 1) - \mathrm{rE}(\lambda)}{\Delta\lambda}, \tag{4}$$

$$\mathrm{DDE} = \frac{\mathrm{DE}(\lambda + 1) - \mathrm{DE}(\lambda)}{\Delta\lambda}, \tag{5}$$

where RE is the reciprocal form of rE, LRE is the logarithm form of RE, DE is the first-order derivative of rE, and DDE is the second-order derivative of rE.

2.3 *Modeling Approach*

As the spectra have a large amount of redundant information of self-similarity, it is necessary to select relevant bands for PLSR models based on a stepwise regression approach, which is a systematic method for adding and removing terms from a polynomial regression in view of statistical significance.[15,44] Band selection is a necessary process for building up a PLSR model with good predictive ability.

After the above process, several bands were chosen for modeling soil water content, and there is still a substantial risk of overfitting in empirical model. Cross-validation is therefore employed to determine the number of components by minimizing the predicted residual sums of squares (PRESS).[45] Leave-p-out cross-validation approach, which involves using p observations as the validation set and the rest as the training set,[46] is performed in this study. The method is to test the predictive significance of each PLSR component and find the best number of components.[34]

PLSR is generally a multivariate regression method that specifies a linear relationship between numerous dependent variables (Y) and predictor variables (X).[47] The approach is effective to reduce collinear spectral data to a few noncorrelated principal components (PCs), which represents the relevant structural information. The performance of PLSR model is evaluated with the determination coefficient (R^2) and root mean square error (RMSE) between measured and estimated soil water content values. An effective model should have a high R^2 and small RMSE.

3 Results

3.1 *Descriptions of Soil Water Content and Spectra*

A total of 150 results of soil water content were collected from five measurements, and soil water content ranged approximately from 0 to 16% [Fig. 1(A)], which were sufficient to represent the actual situation in the arid area. Meanwhile, the relative emissivity was also collected according to each soil water measurement [Fig. 1(B)]. The soil water content varied differently in the former four times measurements, and also the relative emissivity changed greatly. This might be caused by various soil water content, soil particle size, and soil salt motion state, whereas samples had similar soil water content for the last measurement, and the relative emissivity fluctuated in a small range as well.

Due to various soil column sample heights under the same evaporation conditions, different soil salinities finally emerged on sample surface, and soil water content was similar and <2.4% at the last measurement [Fig. 1(A)]. Considering the last measurement as the example, Fig. 2(a) showed the emissivity of all samples (gray) and the average value of each particle size (color). Over 8 to 9.5 μm soil emissivity showed a decreasing trend with the increase in amount of salt. Figures 2(b)–2(d) showed the emissivity of fine, medium, and coarse soil particle size. The results clearly indicated that the emissivity showed small variances among various sample heights and soil particles. This may have been caused by excessively dispersed salt on the

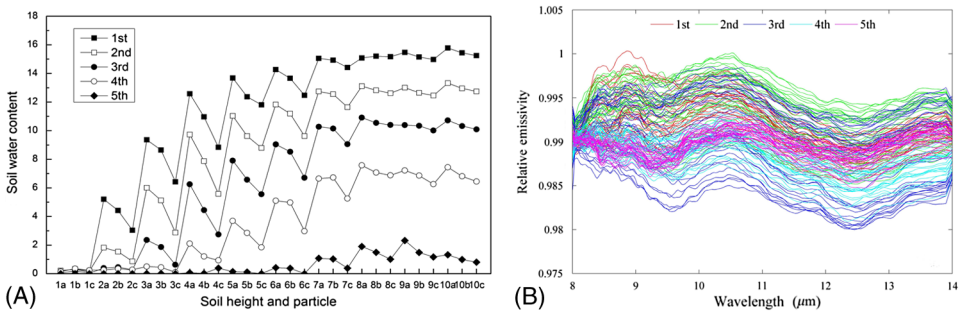

Fig. 1 (A) Soil water content of each sample in evaporation process. The number label of *x* axis represents the height and the letter represents three particles of (a) 0 to 0.2 mm, (b) 0.2 to 2 mm, and (c) >2 mm, respectively. (B) Soil relative emissivity corresponding to soil water content.

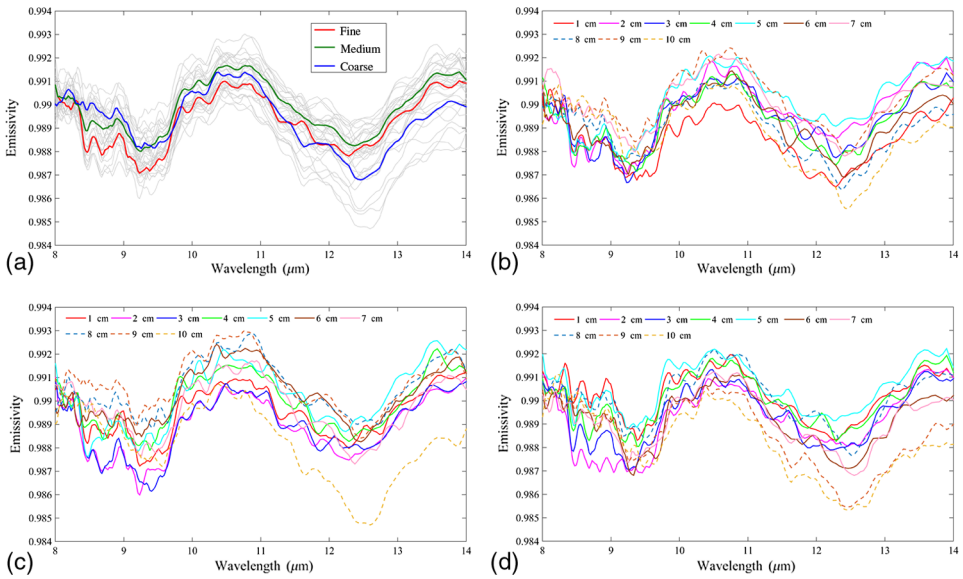

Fig. 2 (a) Sample emissivity (gray) and mean emissivity (color) of each particle size; (b), (c), and (d) represent soil emissivity of fine, medium, and coarse particles at the last measurement.

soil surface. However, at the domain of 8 to 9.5 μm, emissivity of Figs. 2(b) and 2(c) decreased basically with the increasing salt content, while emissivity of Fig. 2(d) showed a similar trend except sample with 1 cm, which was similar to the previous study.[48] This may have been attributable to salinity of the coarse particle sample that could not provide enough salt to cover the soil surface, and hence uncovering sand would increase its emissivity. The rest of the wavelengths showed a controversial pattern. Overall, in view of Figs. 1(B) and 2, soil water content affected emissivity greater than soil salt content, and various salt amounts on soil surface made slight difference on soil emissivity.

3.2 *Correlations Between Soil Water Content and Spectral Forms*

Four spectral forms (rE, LRE, DE, and DDE) were examined here to reveal the relationship between soil water content and transformed spectra (Fig. 3). The correlation regression with four transformed spectra could uncover the subtle spectral features contributing to the soil water content estimation. Absolute values of correlation coefficient of four spectral forms were collected to find important spectral features.

Among the different processing algorithms, largest correlation coefficients found in rE, LRE, DE, and DDE were 0.77, 0.77, 0.71, and 0.69 in turn and located at 8.835, 8.835, 8.747, and 8.813 μm, respectively. In addition, 12 largest coefficients were collected here to identify the effective band domain. The band range of spectral form rE and LRE were both 8.79 to 9.09 μm, while band range of spectral form DE and DDE were 8.08 to 11.15 μm and 8.43 to 11.01 μm, respectively.

We thus conclude that the peak of correlation coefficient had minimal difference for four spectral forms and located at adjacent bands. The sensitive band domains of spectral form DE and DDE were a little wider than that of rE and LRE.

3.3 *Modeling*

Stepwise regression analysis was first carried out based on raw data and soil water content, and finally seven bands were chosen for PLSR model (Table 3). The number of components for PLSR model was determined with cross-validation [Fig. 4(a)]. The PRESS of the training

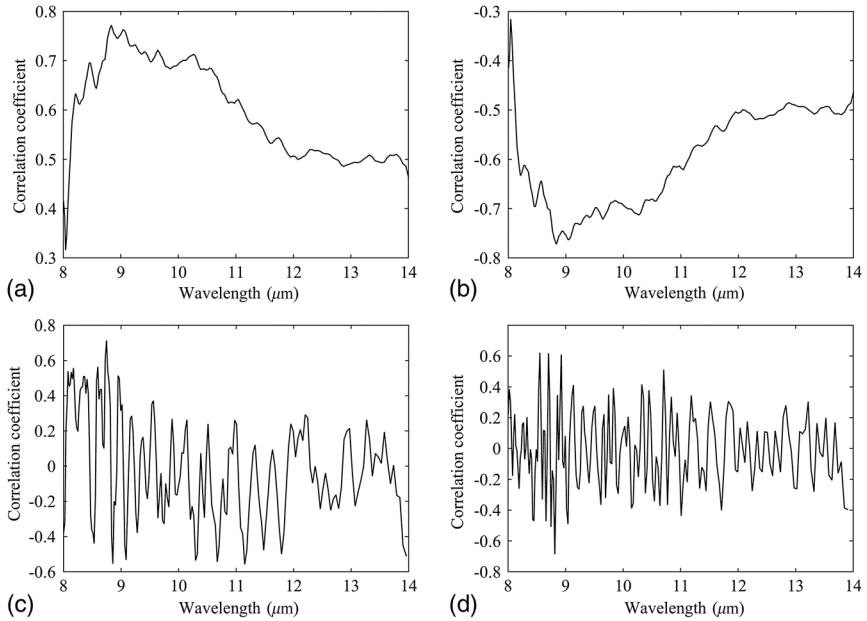

Fig. 3 Correlation coefficient between soil water content and each spectral form: (a) relative emissivity (rE), (b) logarithm of reciprocal spectra (LRE), (c) first-order derivative spectra (DE), and (d) second-order derivative spectra (DDE).

Table 3 Model coefficients of relative bands for four spectral forms.

		Wavelength (μm)									
rE	Intercept	8.813	8.533	8.309	8.791	8.835	8.926	9.112			
Coefficients	−235.76	29,583.6	−1679.61	−1330.42	−12,626.62	−15,293.77	2954.87	−1366.34			
		Wavelength (μm)									
LRE	Intercept	8.813	8.533	8.309	8.791	8.835	8.926	9.112			
Coefficients	6.00	−67,406.45	3835.49	3034.33	28,753.17	34,850.45	−6751.14	3123.66			
		Wavelength (μm)									
DE	Intercept	8.725	8.617	8.329	10.640	9.588	9.065	10.512	8.270	10.771	
Coefficients	0.52	271.6	175.1	109.1	−304.9	215.0	−212.1	−109.1	87.3	−196.23	
		Wavelength (μm)									
DDE	Intercept	8.791	8.747	9.018	10.673	13.218	8.533	10.805	11.186	13.168	13.577
Coefficients	5.07	−8.42	−4.03	−3.71	20.48	−24.54	2.19	12.09	18.54	21.70	−25.17

Note: rE, relative emissivity; LRE, logarithm of reciprocal spectra; DE, first-order derivative spectra; DDE, second-order derivative spectra.

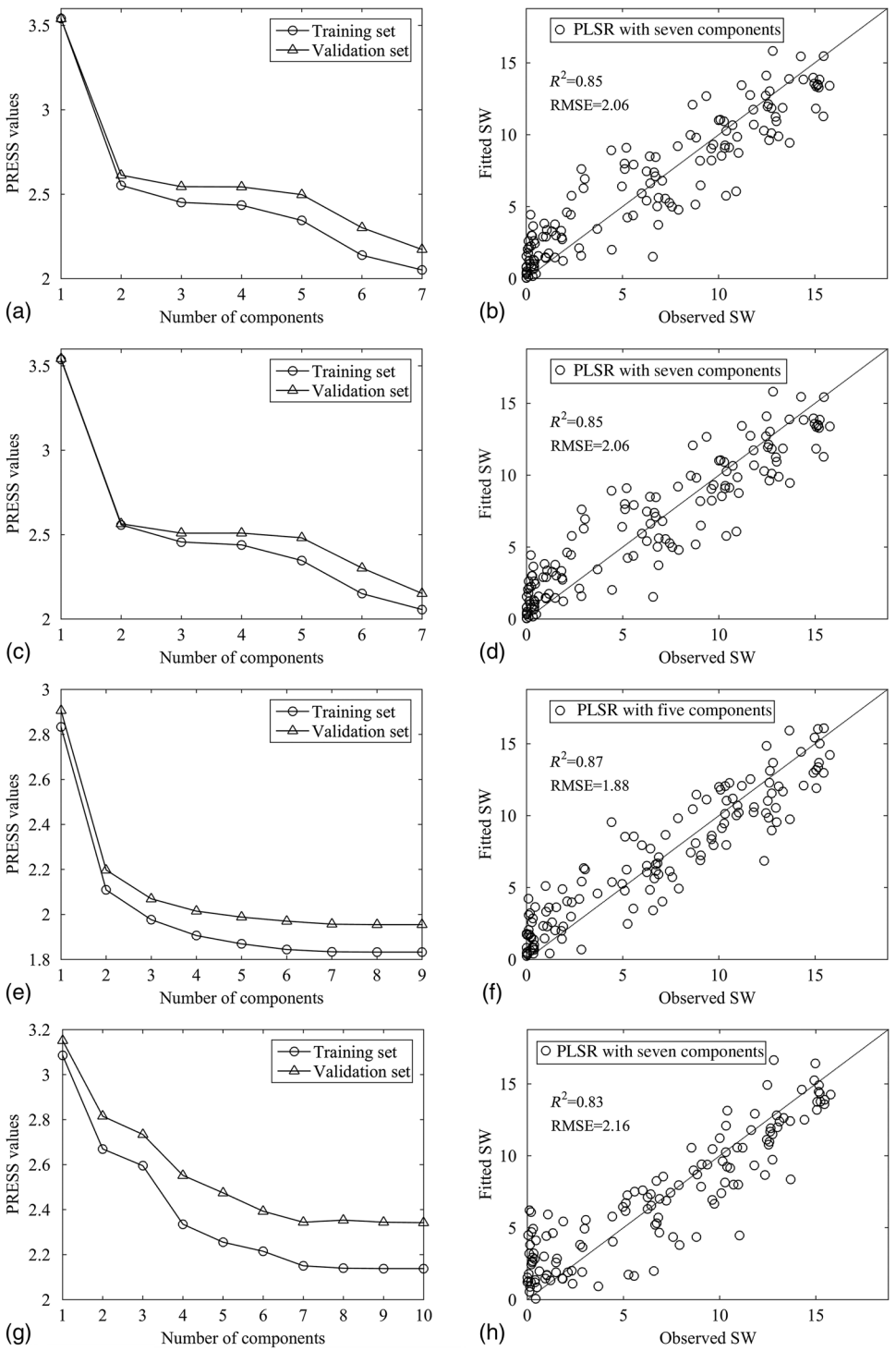

Fig. 4 The result of cross-validation for principal component numbers determination based on rE, LRE, DE, and DDE [(a1), (b1), (c1), and (d1)], and soil water content estimate based on rE, LRE, DE, and DDE [(a2), (b2), (c2), and (d2)].

set and validation set had similar trends, decreasing monotonically with the number of components. Seven components were hence selected to establish the PLSR model for soil water content prediction. Table 3 listed the coefficients of seven bands for the PLSR model. The model for soil water estimation selected all the seven components and performed well for predicting soil water content based on raw spectra. The determination coefficient (R^2) was 0.85 and the RMSE was 2.06% [Fig. 4(b)].

Likewise, the same methods were applied based on the spectral form LRE, and the same performance was obtained as shown in Figs. 4(c) and 4(d). The same bands were also chosen by stepwise regression analysis and illustrated in Table 3. Cross-validation results show that seven components were the best choice for PLSR analysis. The PLSR model predicted soil water content with the same determination coefficient ($R^2 = 0.85$) and RMSE = 2.06% based on LRE spectra as rE spectra.

Different results were obtained from the same method based on spectral form DE. Nine bands (Table 3) were chosen by stepwise regression analysis, and five components were used from PRESS changes. Finally, an effective model was produced with $R^2 = 0.87$ and RMSE = 1.88% [Figs. 4(e) and 4(f)]. The spectral form DDE was dealt with in the same way. Ten bands were chosen from stepwise regression analysis and seven components were determined from the PRESS curve [Table 3 and Fig. 4(g)]. Ultimately, the model was determined with $R^2 = 0.83$ and RMSE = 2.16% [Fig. 4(h)].

From the above four types of spectral forms, we can see that rE and LRE have the same performance for predicting soil water content with PLSR model. And the effective was almost concentrated around 8.309 to 9.112 μm. The spectral form DE performed well with the same means, and got the highest R^2 and least RMSE. Moreover, it involved a wide band domain with 8.270 to 10.771 μm. Although spectral form DDE had minimal weakness for soil water content prediction, a broader band range was involved from 8.533 to 13.577 μm.

4 Discussion

4.1 *Sensitive Bands Determination*

Numerous studies are available on soil water content estimation based on visible-near-infrared and microwave characteristics,[30,49–51] while few studies relate soil water content with far-infrared band.[52] Moreover, far-infrared spectra have been used in estimating soil sand content, organic matter, and surface temperature retrieval.[40,53,54] Numerous statistical regression approaches were conducted for their pros and cons to predict soil spectral properties.[33,55] The PLSR is commonly applied for its robustness.[34] High collinear full-band resulted in difficult selection of real relevant bands for building up PLSR model. Stepwise regression analysis was hence performed to select the bands for PLSR model, instead of using the total domain from 8 to 14 μm. In addition, commonly used spectral pretreatments, such as the first-order derivative, have practical superiority over raw spectra,[30] which agreed with the results in this study.

To further determine the most contributing bands, we identified high numerical values of loading weights for PLSR model. High values implied high importance of the band in PLSR analysis.[56] Loading weights of four spectral forms (rE, LRE, DE, and DDE) over bands for latent variables are shown in Tables 4–7, respectively. For spectral forms rE and LRE, all of the seven bands (range from 8.309 to 9.112 μm) had much higher contribution

Table 4 Loading weight matrix (LW, $\times 10^{-2}$) of each band for the partial least square regression (PLSR) model based on the rE spectra to estimate soil water content.

Band (μm)	PC1	PC2	PC3	PC4	PC5	PC6	PC7
8.813	**4.08**	0.21	0.17	−0.03	−0.03	0.05	0.01
8.533	**3.28**	−0.59	0.13	−0.33	0.13	−0.03	0.00
8.309	**2.69**	−0.61	0.05	0.31	−0.14	0.04	0.00
8.791	**4.04**	0.18	0.15	0.04	0.02	0.04	−0.12
8.835	**4.04**	0.19	0.13	−0.06	−0.09	−0.04	0.09
8.926	**3.92**	0.08	−0.18	0.15	0.18	−0.14	0.05
9.112	**4.07**	0.09	−0.41	−0.03	−0.09	0.08	−0.03

Table 5 Loading weight matrix (LW, $\times 10^{-2}$) of each band for the PLSR model based on the LRE spectra to estimate soil water content.

Band (μm)	PC1	PC2	PC3	PC4	PC5	PC6	PC7
8.813	**−1.78**	−0.09	−0.07	0.01	0.01	−0.02	−0.01
8.533	**−1.43**	0.26	−0.06	0.14	−0.06	0.01	0.00
8.309	**−1.18**	0.27	−0.02	−0.14	0.06	−0.02	0.00
8.791	**−1.77**	−0.08	−0.06	−0.02	−0.01	−0.02	0.05
8.835	**−1.77**	−0.08	−0.06	0.03	0.04	0.02	−0.04
8.926	**−1.71**	−0.04	0.08	−0.07	−0.08	0.06	−0.02
9.112	**−1.78**	−0.04	0.18	0.01	0.04	−0.04	0.01

Table 6 Loading weight matrix (LW, $\times 10^{-2}$) of each band for the PLSR model based on the DE spectra to estimate soil water content.

Band (μm)	PC1	PC2	PC3	PC4	PC5
8.725	**8.52**	**4.69**	−3.92	−2.66	3.99
8.617	2.28	3.72	**4.51**	−1.65	**−4.45**
8.329	**9.63**	−2.95	−2.77	**6.34**	**−5.77**
10.640	−2.15	0.02	−1.76	−0.64	−0.35
9.588	−1.60	2.91	1.64	2.90	1.22
9.065	−2.61	−2.15	−0.02	−0.76	−0.56
10.512	−0.04	0.53	0.76	−0.55	−0.92
8.270	**9.25**	**−6.86**	**5.23**	−3.64	3.40
10.771	−0.30	−1.65	−0.73	−1.56	0.05

Table 7 Loading weight matrix of each band for the PLSR model based on the DDE spectra to estimate soil water content.

Band (μm)	PC1	PC2	PC3	PC4	PC5	PC6	PC7
8.791	**−2.65**	−0.48	**−1.94**	0.15	0.80	−0.08	0.01
8.747	−0.03	**−1.89**	**2.34**	−0.37	0.23	−0.01	−0.02
9.018	**−1.58**	−0.21	−0.23	**1.07**	**−1.89**	−0.08	0.06
10.673	0.43	−0.02	0.04	0.36	0.03	0.19	−0.04
13.218	−0.03	0.00	−0.01	−0.04	−0.05	0.03	−0.24
8.533	**3.46**	−0.96	**−1.59**	0.55	−0.28	−0.08	0.02
10.805	0.23	0.32	0.28	0.13	0.46	−0.78	0.18
11.186	0.00	0.25	−0.17	0.38	−0.06	0.44	−0.24
13.168	0.13	0.02	−0.06	0.08	0.04	0.07	−0.02
13.577	−0.06	−0.01	−0.05	0.05	−0.04	−0.01	−0.19

Table 8 Thermal infrared bands of available and frequently used satellites.

Sensor	Satellite	Band (μm)	Spatial resolution (m)
ASTER	EOS	8.125 to 8.475, 8.925 to 9.275, 10.25 to 10.95, 8.475 to 8.825, 10.95 to 11.65	90
MODIS	EOS	8.4 to 8.7, 9.58 to 9.88, 10.78 to 11.28, 13.185 to 13.485, 13.785 to 14.085, 11.77 to 12.27, 13.485 to 13.785, 14.085 to 14.385	1000

for PC1 than other components (described by bold numbers, similarly hereinafter). For DE spectra, although the involved band was wide from 8.27 to 10.771 μm, only four bands (range from 8.27 to 9.725 μm) contributed a lot to five PCs. As for DDE spectra, a broad band domain from 8.533 to 13.577 μm was involved, but only regions from 8.533 to 9.018 μm gave the major contribution. We hence concluded that 8.27 to 9.112 μm was the dominant band range for PLSR model to estimate soil water content.

4.2 *Possibility of Soil Salt Content Estimation*

Although many researchers reported the potential of far-infrared to distinguish and quantify soil organic matter, temperature, water, composition, and other materials,[53,57–59] few studies have been conducted to estimate soil salt content using far-infrared wavelength. There are still a few studies of elemental analysis of basic salinity, which find that bending vibration band of nitrate and carbonate is located around 7.4 and 6.89 μm[60,61] using an attenuated total reflection spectroscopy. Xia et al.[48] measured soil emissivity and soil salt content randomly at the same time in a field. To estimate soil salt content, soil samples with different levels of soil salt content should be arranged experimentally, where various soil salt contents and their corresponding emissivity are measured when modeling salt content. Soil water content and other complex factors impact soil emissivity in the field experiment, but the robustness of models would be largely improved for estimating a certain soil variable without regard to the others.[30]

4.3 *Potential Applications at Large Scale*

Currently, there are many satellite sensors containing far-infrared bands, for example, ASTER, AVHRR, MODIS, Landsat ETM+, and so on, and especially ASTER and MODIS have more channels in far-infrared band region (Table 8). The chosen bands from rE and LRE spectral forms had the best accuracy for soil water content prediction and only covered three corresponding bands of ASTER sensor and one band of MODIS sensor. DE spectra form also covered four bands of ASTER sensor and two bands of MODIS sensor. Although the DDE spectral form did not perform very well, it involves four bands of ASTER and MODIS sensor. This might be advantageous to provide good estimates of soil characteristics for widespread use at large scales, which should be considered in future studies.

However, spectral resolution of satellite sensor is much broader than the instrument used in this study, which may influence the accuracy of the soil property estimation at large scale. Liang has attempted successfully to convert narrowband to broadband albedo and established a series of conversion formulae based on extensive radiative transfer simulations,[62] and extensive field measurements have been conducted to validate these formulae for a series of sensors.[63] In view of this, there is a chance of converting bands mentioned in the current result to broadband of the sensors with the processing approach.

On the other hand, the field condition is very complex and contains many factors that may not be fully captured in the lab experiment, such as soil mineralogy, texture, organic carbon, and various species of vegetation.[4] Despite all that, some progresses have been made on visible/near-infrared and thermal infrared data, which will be helpful for large-scale application by combining some other variables, like temperature, NDVI, and thermal inertia.[11,14] The influence of soil water content on far-infrared emissivity is a known fact but has been poorly studied in the past,[64] and the influence of other factors for estimating soil water content will also be studied

in future work. In addition, the most contribution band region concentrated on 8.27 to 9.112 μm, which should be considered to design future thermal sensors to accommodate the request.

5 Conclusions

Spectral estimate of soil water content was presented in this study, and the possibilities of far-infrared band domain were validated to quantitatively derive soil water content of salt-affected soil in arid regions. PLSR analysis was applied to verify statistical relationships between soil water content and four spectral forms (rE, LRE, DE, and DDE). Among the four types of spectral form, DE was identified as the most potential spectral form, and the predictive result was achieved with an R^2 of 0.87 and an RMSE of 1.88%, while model with DDE covered the widest range from 8.533 to 13.577 μm with a little less accuracy ($R^2 = 0.83$ and RMSE = 2.16%). Judging from the contribution of bands to each PC, we suggest that 8.27 to 9.112 μm region is best for delineating soil water content with high prediction accuracy. Although there are still many constraints for large-scale application, the result also demonstrated that far-infrared data were helpful for predicting soil water content and also provided meaningful insights and a prerequisite for designing thermal sensors in future.

Acknowledgments

This study was financially supported by funds from the Chinese Academy of Sciences action-plan for West Development under Grant No. KZCX2-XB-16, the State Key Program for Basic Research of China under Grant No. 2015FY110500 and the National Basic Research Program of China under Grant No. 2015CB150802. We thank Professor Wang Quan and the staff at Wulanwusu Agrometeorological Experiment Station for their facilities and support.

References

1. J. P. Wigneron et al., "Use of passive microwave remote sensing to monitor soil moisture," *Agronomie* **18**(1), 27–43 (1998).
2. K. Z. Mganga et al., "The role of moisture in the successful rehabilitation of denuded patches of a semi-arid environment in Kenya," *J. Environ. Sci. Technol.* **3**(4), 195–207 (2010).
3. A. L. Kaleita, L. F. Tian, and M. C. Hirschi, "Relationship between soil moisture content and soil surface reflectance," *Trans. ASAE* **48**(5), 1979–1986 (2005).
4. W. Hendrik et al., *Remote Sensing of Soils*, University of Zurich, Switzerland (2014).
5. P. Rahimzadeh-Bajgiran et al., "Estimation of soil moisture using optical/thermal infrared remote sensing in the Canadian Prairies," *ISPRS J. Photogramm. Remote Sens.* **83**, 94–103 (2013).
6. E. M. Dante and P. S. Dhruba, "The use of hyperspectral data in identifying 'desert-like' soil surface features in Tabernas area, southeast Spain," in *22nd Asian Conf. on Remote Sensing*, pp. 5–9 (2001).
7. E. L. Skidmore, J. D. Dickerson, and H. Schimmelpfennig, "Evaluating surface-soil water-content by measuring reflectance," *Soil Sci. Soc. Am. J.* **39**(2), 238–242 (1975).
8. S. A. Bowers and R. J. Hanks, "Reflection of radiant energy from soils," *Soil Sci.* **100**(2), 130–138 (1965).
9. H. Li et al., "Predicting water content using linear spectral mixture model on soil spectra," *J. Appl. Remote Sens.* **7**, 073539 (2013).
10. K. Richter et al., "Evaluation of near-surface soil water status through the inversion of soil-canopy radiative transfer models in the reflective optical domain," *Int. J. Remote Sens.* **33**(17), 5473–5491 (2012).
11. M. Minacapilli, M. Iovino, and F. Blanda, "High resolution remote estimation of soil surface water content by a thermal inertia approach," *J. Hydrol.* **379**(3–4), 229–238 (2009).
12. D. L. Neema, A. Shah, and A. N. Patel, "A statistical optical-model for light-reflection and penetration through sand," *Int. J. Remote Sens.* **8**(8), 1209–1217 (1987).

13. M. S. Moran et al., "Estimating crop water-deficit using the relation between surface-air temperature and spectral vegetation index," *Remote Sens. Environ.* **49**(3), 246–263 (1994).
14. R. R. Gillies et al., "A verification of the 'triangle' method for obtaining surface soil water content and energy fluxes from remote measurements of the normalized difference vegetation index (NDVI) and surface radiant temperature," *Int. J. Remote Sens.* **18**(15), 3145–3166 (1997).
15. W. D. Liu et al., "Relating soil surface moisture to reflectance," *Remote Sens. Environ.* **81**(2–3), 238–246 (2002).
16. M. L. Whiting, L. Li, and S. L. Ustin, "Predicting water content using Gaussian model on soil spectra," *Remote Sens. Environ.* **89**(4), 535–552 (2004).
17. T. J. Jackson et al., "Soil moisture mapping at regional scales using microwave radiometry: the Southern Great Plains hydrology experiment," *IEEE Trans. Geosci. Remote Sens.* **37**(5), 2136–2151 (1999).
18. T. Zhang et al., "Effects of spatial distribution of soil parameters on soil moisture retrieval from passive microwave remote sensing," *Sci. China Earth Sci.* **55**(8), 1313–1322 (2012).
19. J. R. Wang and T. J. Schmugge, "An empirical-model for the complex dielectric permittivity of soils as a function of water-content," *IEEE Trans. Geosci. Remote Sens.* **GE-18**(4), 288–295 (1980).
20. T. J. Jackson and T. J. Schmugge, "Passive microwave remote-sensing system for soil-moisture—some supporting research," *IEEE Trans. Geosci. Remote Sens.* **27**(2), 225–235 (1989).
21. R. Bindlish and A. P. Barros, "Subpixel variability of remotely sensed soil moisture: an inter-comparison study of SAR and ESTAR," *IEEE Trans. Geosci. Remote Sens.* **40**(2), 326–337 (2002).
22. K. B. Mao et al., "A method for retrieving soil moisture in Tibet region by utilizing microwave index from TRMM/TMI data," *Int. J. Remote Sens.* **29**(10), 2903–2923 (2008).
23. L. Raphael, "Application of FTIR spectroscopy to agricultural soils analysis," Chapter 18 in *Fourier Transforms—New Analytical Approaches and FTIR Strategies*, G. Nikolic, Ed., pp. 385–404, InTech, Israel (2011).
24. T. N. Carlson, W. J. Capehart, and R. R. Gillies, "A new look at the simplified method for remote-sensing of daily evapotranspiration," *Remote Sens. Environ.* **54**(2), 161–167 (1995).
25. T. N. Carlson, R. R. Gillies, and T. J. Schmugge, "An interpretation of methodologies for indirect measurement of soil-water content," *Agric. For. Meteorol.* **77**(3–4), 191–205 (1995).
26. I. Sandholt, K. Rasmussen, and J. Andersen, "A simple interpretation of the surface temperature/vegetation index space for assessment of surface moisture status," *Remote Sens. Environ.* **79**(2–3), 213–224 (2002).
27. W. Wang et al., "Estimation of soil moisture using trapezoidal relationship between remotely sensed land surface temperature and vegetation index," *Hydrol. Earth Syst. Sci.* **15**(5), 1699–1712 (2011).
28. F. Csillag, L. Pasztor, and L. L. Biehl, "Spectral band selection for the characterization of salinity status of soils," *Remote Sens. Environ.* **43**(3), 231–242 (1993).
29. J. Farifteh, "Interference of salt and moisture on soil reflectance spectra," *Int. J. Remote Sens.* **32**(23), 8711–8724 (2011).
30. Q. Wang et al., "Calibration and validation of salt-resistant hyperspectral indices for estimating soil moisture in arid land," *J. Hydrol.* **408**(3–4), 276–285 (2011).
31. J. Farifteh, F. van der Meer, and E. J. M. Carranza, "Similarity measures for spectral discrimination of salt-affected soils," *Int. J. Remote Sens.* **28**(23), 5273–5293 (2007).
32. Y. L. Weng, P. Gong, and Z. L. Zhu, "Soil salt content estimation in the Yellow River delta with satellite hyperspectral data," *Can. J. Remote Sens.* **34**(3), 259–270 (2008).
33. W. A. Dorigo et al., "A review on reflective remote sensing and data assimilation techniques for enhanced agroecosystem modeling," *Int. J. Appl. Earth Obs. Geoinf.* **9**(2), 165–193 (2007).
34. S. Wold, M. Sjostrom, and L. Eriksson, "PLS-regression: a basic tool of chemometrics," *Chemometr. Intell. Lab. Syst.* **58**(2), 109–130 (2001).

35. W. Geyer, L. Brüggemann, and G. Hanschmann, "Prediction of properties of soil humic substances from FTIR spectra using partial least squares regression," *Int. J. Environ. Anal. Chem.* **71**(2), 181–193 (1998).
36. L. Li, "Partial least squares modeling to quantify lunar soil composition with hyperspectral reflectance measurements," *J. Geophys. Res. Planet* **111**(E4), E04002 (2006).
37. Z. Huang et al., "Estimating foliage nitrogen concentration from HYMAP data using continuum removal analysis," *Remote Sens. Environ.* **93**(1–2), 18–29 (2004).
38. A. M. Rady et al., "The potential use of visible/near infrared spectroscopy and hyperspectral imaging to predict processing-related constituents of potatoes," *J. Food Eng.* **135**, 11–25 (2014).
39. E. M. Abdel-Rahman et al., "A comparison of partial least squares (PLS) and sparse PLS regressions for predicting yield of Swiss chard grown under different irrigation water sources using hyperspectral data," *Comput. Electron. Agric.* **106**, 11–19 (2014).
40. M. Sawut et al., "Estimating soil sand content using thermal infrared spectra in arid lands," *Int. J. Appl. Earth Obs. Geoinf.* **33**(0), 203–210 (2014).
41. G. P. Luo et al., "Temporal and spatial variation and stability of the oasis in the Sangong River watershed, Xinjiang, China," *Sci. China Ser. D* **46**(1), 62–73 (2003).
42. Designs & Prototypes, "D&P instruments," http://www.dpinstruments.com.
43. C. Y. Wu et al., "Accounting for surface roughness effects in the near-infrared reflectance sensing of soils," *Geoderma* **152**(1–2), 171–180 (2009).
44. R. I. Jennrich and P. F. Sampson, "Application of stepwise regression to non-linear estimation," *Technometrics* **10**(1), 63 (1968).
45. S. Chen et al., "Sparse modeling using orthogonal forward regression with PRESS statistic and regularization," *IEEE Trans. Syst. Man Cybern. Part B Cybern.* **34**(2), 898–911 (2004).
46. J. Shao, "Linear-model selection by cross-validation," *J. Am. Stat. Assoc.* **88**(422), 486–494 (1993).
47. D. M. Haaland and E. V. Thomas, "Partial least-squares methods for spectral analyses. 2. Application to simulated and glass spectral data," *Anal. Chem.* **60**(11), 1202–1208 (1988).
48. J. Xia et al., "Application study of the thermal infrared emissivity spectra in the estimation of salt content of saline soil," *Spectrosc. Spectral Anal.* **32**(11), 2956–2961 (2012).
49. D. B. Lobell, "Moisture effects on soil reflectance," *Soil Sci. Soc. Am. J.* **66**(3), 722–727 (2002).
50. C. S. Ruf and H. P. Zhang, "Performance evaluation of single and multichannel microwave radiometers for soil moisture retrieval," *Remote Sens. Environ.* **75**(1), 86–99 (2001).
51. M. Parde et al., "Soil moisture estimations based on airborne CAROLS L-band microwave data," *Remote Sens.* **3**(12), 2591–2604 (2011).
52. A. Lesaignoux, S. Fabre, and X. Briottet, "Influence of soil moisture content on spectral reflectance of bare soils in the 0.4-14 μm domain," *Int. J. Remote Sens.* **34**(7), 2268–2285 (2013).
53. R. R. E. Artz et al., "FTIR spectroscopy can be used as a screening tool for organic matter quality in regenerating cutover peatlands," *Soil Biol. Biochem.* **40**(2), 515–527 (2008).
54. H. Ren et al., "Angular normalization of land surface temperature and emissivity using multiangular middle and thermal infrared data," *IEEE Trans. Geosci. Remote Sens.* **52**(8), 4913–4931 (2014).
55. S. Nawar et al., "Modeling and mapping of soil salinity with reflectance spectroscopy and landsat data using two quantitative methods (PLSR and MARS)," *Remote Sens.* **6**(11), 10813–10834 (2014).
56. P. M. Hansen and J. K. Schjoerring, "Reflectance measurement of canopy biomass and nitrogen status in wheat crops using normalized difference vegetation indices and partial least squares regression," *Remote Sens. Environ.* **86**(4), 542–553 (2003).
57. J. W. Salisbury and D. M. Daria, "Infrared (8-14 μm) remote-sensing of soil particle-size," *Remote Sens. Environ.* **42**(2), 157–165 (1992).
58. M. Tatzber et al., "An alternative method to measure carbonate in soils by FT-IR spectroscopy," *Environ. Chem. Lett.* **5**(1), 9–12 (2007).
59. M. Mira et al., "Soil moisture effect on thermal infrared (8-13-μm) emissivity," *IEEE Trans. Geosci. Remote Sens.* **48**(5), 2251–2260 (2010).

60. A. Shaviv et al., "Direct monitoring of soil and water nitrate by FTIR based FEWS or membrane systems," *Environ. Sci. Technol.* **37**(12), 2807–2812 (2003).
61. R. Linker et al., "Soil identification and chemometrics for direct determination of nitrate in soils using FTIR-ATR mid-infrared spectroscopy," *Chemosphere* **61**(5), 652–658 (2005).
62. S. Liang, "Narrowband to broadband conversions of land surface albedo I: algorithms," *Remote Sens. Environ.* **76**(2), 213–238 (2001).
63. S. Liang et al., "Narrowband to broadband conversions of land surface albedo: II. Validation," *Remote Sens. Environ.* **84**(1), 25–41 (2003).
64. M. Mira et al., "Influence of soil water content on the thermal infrared emissivity of bare soils: implication for land surface temperature determination," *J. Geophys. Res. Earth Surf.* **112**(F4), F04003 (2007).

Lu Xu is a doctoral student at the Institute of Xinjiang Institute of Ecology and Geography, CAS. His current research interests are hyperspectral remote sensing of soil moisture, salinity, and physical parameters of salt-affected soil.

Zhichun Wang is a professor at Northeast Institute of Geography and Agroecology, CAS. He is engaged in monitoring and amelioration of saline soil and research of soil ecology and plant nutrition.

Maina John Nyongesah holds a PhD in ecology from the Institute of Xinjiang Institute of Ecology and Geography, CAS. He is currently a university lecturer in Kenya, and his current research is remote retrieval of ecosystem biosphysical and physiological properties of vegetation with keen interest in species adaptation to climate change.

Gang Liu is a PhD graduate from the Graduate School of Agriculture, Shizuoka University, Shizuoka, Japan. His current research is ecosystem gas flux on transects with interest in fragile ecosystem response to climate change.